Method to Increase WPTS Robustness to Frequency Splitting and Bifurcation Phenomena

Damien Lemaitre, Benoît Sarrazin, Yohan Wanderoild, Alexis Derbey, Thierry Brincourt, Yves Lembeye

Method to Increase WPTS Robustness to Frequency Splitting and Bifurcation Phenomena.

Damien Lemaitre[1,2], Benoît Sarrazin[2], Yohan Wanderoild[1], Alexis Derbey[2],
Thierry Brincourt[1], Yves Lembeye[2]

[1]EDF R&D, France
[2]Univ. Grenoble Alpes, CNRS, Grenoble INP, France

Corresponding author: Damien Lemaitre, damien.lemaitre@grenoble-inp.fr

Abstract

Wireless Power Transfer System (WPTS) for electrical vehicle (EV) charging presents many advantages, but the classical values of coupling and load resistance can lead to frequency splitting phenomenon (FSP) and bifurcation phenomenon (BP). The latter affect the system performances due to a potential lower power factor, loss of the zero-voltage switching (ZVS), high sensitivity to over coupling. The present paper provides a method for selecting capacitor values to avoid/reduce these phenomena, specifically allowing to preserve ZVS until an over coupling 67 % higher than classical case.

1 Introduction

The development of electric vehicles (EVs) is leading to a growing need for chargers. EVs are largely charged with plug-in chargers. The safety of no exposed conductor, the galvanic isolation, the resistance to vandalism, weathering and the user comfort make wireless power transfer system (WPTS) attractive. The principle of the WPTS is presented in Fig. 1. The electrical circuit of the system is given in Fig. 2 considering a series-series (SS) resonant topology.
Maximising efficiency is one of the main objectives of WPTS to compete with plug in chargers. One of the main concerns is how to design the coils for a desired power with maximum efficiency considering the all physical parameters, i.e. airgap, compensation topology, coil shape, etc.
In addition, the design procedure becomes more complicated considering Zero Voltage Switching (ZVS), bifurcation and splitting frequency phenomena.
The latter are defined in part 2, where their influence on the system operation is studied.
Part 3 proposes a study to measure the accentuation of bifurcation and frequency splitting according to the values of the coupling coefficient and the load resistance. Considerations used later for the design of the system are defined.
Part 4 proposes a new method to reduce these phenomena and to increase the robustness of the system to coupling and load resistance variations. These results are applied and validated experimentally in part 5.

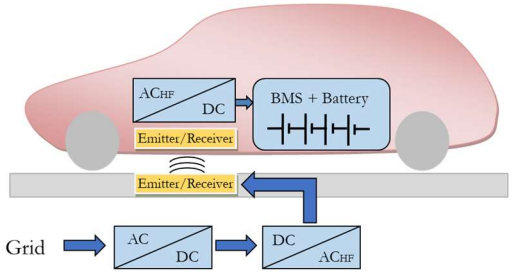

Fig. 1: WPTS principle of an EV charging

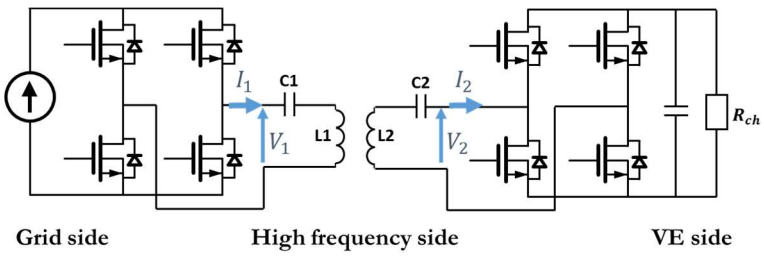

Fig. 2: Schematic of a series-series resonant DC-DC converter

2 Phenomena Description

Looking for highly efficient WPTS lead to consider bifurcation phenomenon (BP) and frequency splitting phenomenon (FSP). These phenomena are however defined differently in the literature, sometimes assimilated, sometimes confused.
The section below provides the definitions of BP and FSP considered in this article. The influence of these phenomena on the system will then be presented.

2.1 Definitions

To begin with, it is necessary to introduce the input phase angle (IPA) φ_1 between the voltage V1 and the current I1 defined in Fig. 2. The frequency where the phase shift φ_1 is equal to zero is called "zero phase angle" (ZPA) frequency. The power factor on the primary side of the coupler PF_1 is the cosine of φ_1 as defined in equation (1). The system therefore has a maximum power factor of 1 when operating at the ZPA frequency. The impedance seen from the source is in fact purely resistive.

$$\mathrm{PF}_1 = \cos(\varphi_1) \qquad (1)$$

Few articles address BP and FSP simultaneously. Several articles in the literature present the bifurcation phenomenon as the occurrence of several ZPA frequencies [1]–[6]. The term “bifurcation” is sometimes used to refer to another phenomenon describing several maximums of the output power as a function of the switching frequency [7], [8].

The occurrence of multiple ZPA frequencies and multiple power peaks is very often linked as we will see in part 3. However, one phenomenon can clearly appear without the other as illustrated in [9]. It is therefore necessary to distinguish these two phenomena.
Following the definition proposed in [9], bifurcation will here refer to the appearance of several output power peaks as a function of the switching frequency, see Fig. 3 (a). The term "frequency splitting" will therefore refer to the occurrence of several ZPA frequencies for the IPA, see Fig. 3 (b).

2.2 Influence on System Performances

The BP and FSP can be more or less pronounced as shown in Fig. 3 (a) Fig. 3 (b). The curves in these figures show the output power and the IPA φ_1 as a function of switching frequency for the same system, sized at a resonant frequency f_r of 81 kHz, for a rated power of 20 kW. The coupling coefficient is different in the three cases shown. The grey, orange and blue curves are obtained for coupling coefficients k of 0.1, 0.135 and 0.25 respectively.
If the BP is sufficiently pronounced, it is possible that the maximums of the output power no longer reach the rated power as illustrated with the blue curve (k=0.25) in Fig. 3 (a). This is a major drawback.
The FSP is problematic because it can cause the loss of the ZVS as illustrated in Fig. 3 (b) by the blue curve (k=0.25). The ZVS mode for the primary side inverter is ensured when operating above the resonant frequency [10]. This requires an inductive impedance seen by the inverter that can be expressed by the condition from equation (2).

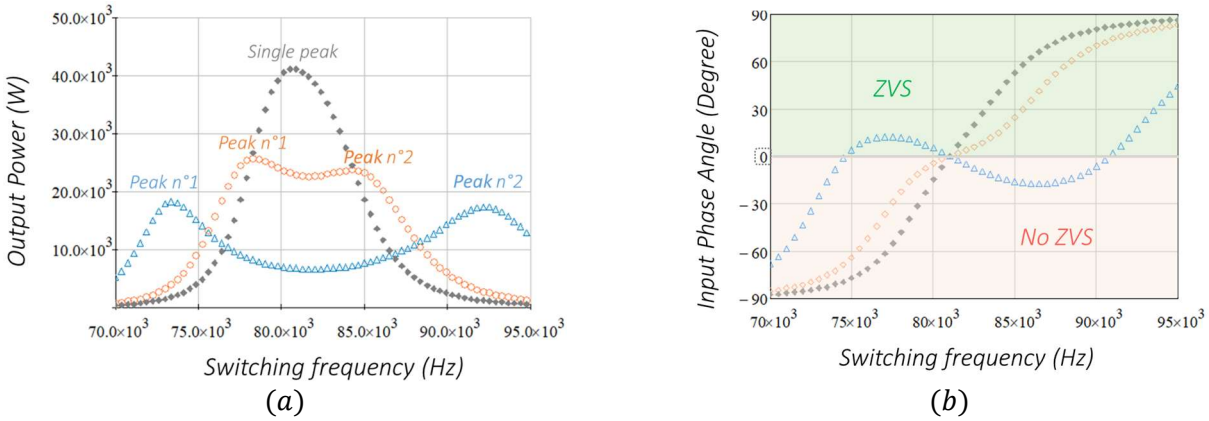

Fig. 3: Illustration of the bifurcation phenomenon (BP) (a) and of the frequency splitting phenomenon (FSP) (b) as function of switching frequency, resulting respectively in two maximums regarding output power and in several ZPA frequencies. These curves are obtained considering a designed WPTS of 20 kW at a resonant frequency f_r equal to 81 kHz, with inductances and resonant capacitances values on primary and secondary side of L_1, L_2, C_1, C_2 respectively equal to 338.74 µH, 80.66 µH, 11.49 nF and 47.86 nF. Coupling coefficient considered for the grey, orange and blue curves are respectively 0.1, 0.135 and 0.25.

$$\varphi_1 = \arg\left(\frac{\overline{V_1}}{\overline{I_1}}\right) > 0 \quad (2)$$

FSP induced several zero-phase angle (ZPA) frequencies and reduced the input phase angle (IPA) value at the nominal point, that can become lower than the minimum value to guarantee ZVS mode. ZVS improves WPTS efficiency and protect the switch from hard switching that can bring over heat if designed for ZVS only. If ZVS can be obtained under FSP and BP, these last make the IPA much more sensitive to coupling variations. The ZVS is then only possible for a very small range of coupling coefficient k. The FSP also induces a decrease in efficiency through a higher IPA at rated power. In addition, several control strategies can become inefficient or less effective due to FSP [4], [11].
The solutions provided in the state of the art to avoid these phenomena are described in the following section.

2.3 Criteria to avoid frequency

The electrical diagram in Fig. 4 is equivalent to the diagram in Fig. 2, considering the expression of Rs defined in (3). The primary quality factor Q_1 and secondary quality factor Q_2 of the system according to the definitions in [12] are given by the equations (4) and (5) respectively.

$$R_s = \frac{8}{\pi^2}.R_{ch} \quad (3)$$

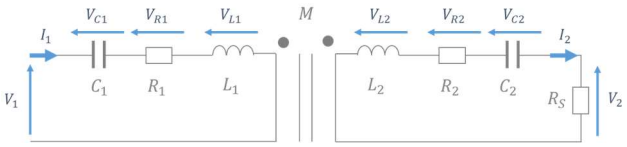

Fig. 4: Equivalent electrical circuit of WPTS.

$$Q_1 = \frac{L_1.R_s}{w_r.M^2} \quad (4)$$

$$Q_2 = \frac{w_r.L_2}{R_s} \quad (5)$$

While the FSP occurrence can be clearly defined through the transition from one to several zero IPA frequencies, BP apparition is harder to define due to a progressive appearance. This is why the criteria for avoiding the FSP as shown in Fig. 3 (b) are predominant in the literature. These are summarised in table 1 of [13] for systems with a SS resonant compensation topology. It should be noted that some of these criteria for avoiding the FSP, contained in equations (6), (7) and (8), are equivalent. The coupling coefficient between the primary and secondary windings of the system is noted k.

The critical coupling coefficient above which the FSP occurs is denoted k_{FSP}.

$$Q_2 < \sqrt{\frac{1}{2.\left(1-\sqrt{1-k^2}\right)}} \quad (6)$$

$$k < k_{FSP} = \frac{1}{Q_2}\sqrt{1-\frac{1}{4.Q_2^2}} \quad (7)$$

$$Q_1 > \frac{4.Q_2^3}{4.Q_2^2-1} \quad (8)$$

These criteria ensure that the operation of the switches in ZVS mode is maintained at the nominal operating point for which the system has been designed. However, they severely restrict the coupling coefficient in the coupler design, which impacts the system efficiency.
Furthermore, choosing to maximize the coupling by taking the coupling coefficient k equal to k_{FSP} defined in equation (7) can be a trade-off between maximizing the coupling coefficient and limiting the accentuation of the BP and FSP.

3 Influential Parameters

The influence of the coupling coefficient and load resistance on the BP and FSP is carried out on a 20 kW WPTS, dimensioned for a resonant frequency of 81 kHz with an air gap of 21 cm. This coupler is presented here [14] and in part 5. The latter has been designed for a coupling coefficient k_d = 0.155, considering primary L1 and secondary L2 inductances of 338.74 µH and 80.66 µH respectively. The theoretical capacitances $C1_{th}$ and $C2_{th}$ calculated according to equation (9) at the resonant frequency are therefore 11.40 nF and 47.86 nF respectively.

$$C_{th} = \frac{1}{4.\pi^2.f_r^2.L} \quad (9)$$

The coupling coefficient of the system obtained under the design conditions, i.e. an air gap of 21 cm and with the windings aligned is noted kd.
It should be noted that the system has been designed such that k_d = k_{FSP} defined in equation (7) in order to maximize the coupling and limit the BP and FSP.

3.1 Coupling Coefficient

The influence of the coupling variation on the power transfer and the input phase angle is clearly illustrated in Fig. 3 (a) Fig. 3 (b). Over-coupling defines the case where k > kd. The larger the coupling k is in front of kd, the more pronounced the BP and FSP are. In contrast, a coupling k < kd reduces these phenomena.

3.2 Charge Resistance

The load resistance is a second parameter with a strong influence on the BP and FSP. The voltage across the EV battery represented by the load resistance Rch varies during charging. Considering that the power transferred to the battery Pout remains constant during charging, this implies that the resistance Rch varies with the charging voltage.

The variation of Rch does not change the power factor PF_1. However, a charging voltage of 350 V, 400 V and 450 V implies charging resistances of 6.1 Ω , 8.0 Ω and 10.1 Ω respectively for a constant charging power of 20 kW. Fig. 5 (a) and (b) show respectively for a coupling coefficient kd = 0.155 the output power and IPA obtained for these three resistance values.

The trend shows that the BP and FSP increase with decreasing Rch, i.e. at the beginning of the battery charge.

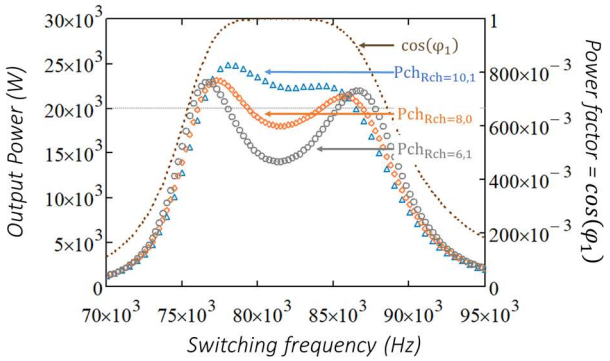

(a)

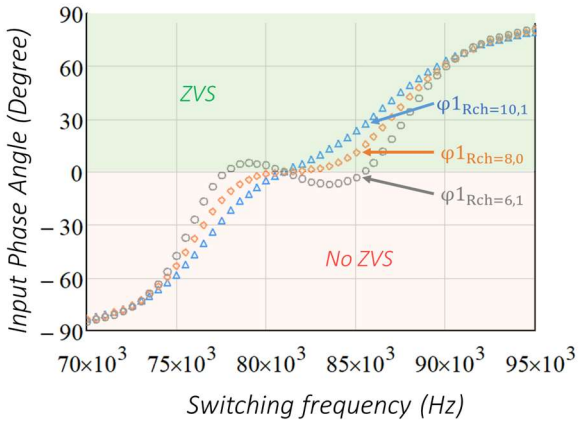

(b)

Fig. 5: Output power transferred (a) and Input phase angle (b) for the load resistances Rch equal to 6.1Ω, 8.0Ω, and 10.1Ω corresponding to grey, orange, and blue curves respectively. Power factor cos(φ_1) is the same for all three cases and illustrated in brown. The coupling is k = 0.155 for the three cases. The WPTS studied has a nominal power of 20 kW, a resonance frequency of 81 kHz.

4 Method proposed

The choice of the capacitance of the primary and secondary resonant capacitors is classically made from equation (9). It is often difficult to obtain in practice the exact values of C1th and C2th due to the limited values of capacitors on the market. The output power vs. frequency curve can vary greatly depending on the choice made for a few percent difference in capacitance as will be detailed later.

The following section proposes to add an additional capacitor selection criterion that provides a significant gain in system robustness to the BP and FSP.

The robustness of the system gained by the proposed method will be studied analytically on the 20 kW system introduced in part 3.

4.1 Description

The proposed sizing method is divided into two steps.

In order to maximize the efficiency while avoiding having pronounced BP and FSP, the first step is to perform the sizing of the WPTS with a coupling not lower than but equal to the critical coupling k_{FSP} given by equation (7). Inductances and resonant capacitances values L_1, L_2, C_1, C_2 are thus obtained on primary and secondary side at the desired resonant frequency f_r, equal here to 81 kHz.

The second step consists in a slight change of resonant capacitance values C1th, C2th. The new capacitance values thus obtained are noted C1c, C2c and are selected according to the classical criterion n°1, to which is added criterion n°2 below. The parameter Xc must be close to 1.

- Criterion n°1: $\mathrm{C1_c} \approx \mathrm{C1_{th}}$ & $\mathrm{C2_c} \approx \mathrm{C2_{th}}$
- Criterion n°2: $\mathrm{C1_c} = \mathrm{X_c}.\frac{\mathrm{L_2}}{\mathrm{L_1}}.\mathrm{C2_c}$, with $\mathrm{X_c} \neq 1$

Criterion 1 ensures a good power factor, necessary to maximise efficiency. Criterion n°2 comes from inequation (10) below and allows the correction of the double resonance seen by the reflected impedance at the primary in the case of BP and FSP.

$$\mathrm{fr_1} = \frac{1}{2.\pi.\sqrt{\mathrm{L_1}.\mathrm{C_{1c}}}} \neq \mathrm{fr_2} = \frac{1}{2.\pi.\sqrt{\mathrm{L_1}.\mathrm{C_{2c}}}} \qquad (10)$$

The influence of the parameter Xc is detailed in the following part, noting that Xc = 1 is the classical case.

4.2 Study on 20 kW WPTS

The robustness of the system gained by the proposed method is studied based on the 20 kW system introduced in part 3.

The comparison between the classical case corresponding to Xc = 1 and the proposed method is made according to three criteria: the ability of the system to transfer its nominal output power $\mathrm{Pout_d}$, its ability to operate in ZVS mode, and its power factor. These three parameters are studied for different coupling coefficients k. The ZVS operation and power factor are calculated at the nominal output power for each value of k. The coupling coefficient varies according to the distance between the windings as well as their misalignment.

Capacitance values C1c and C2c of case Xc > 1 of the proposed solution is the one used during the experimental validation of the method in part 5, hence this choice for the theoretical comparison. The values chosen are C1c = 12.5 nF and C2c = 50 nF, which corresponds to Xc = 1.041. The second proposed case Xc < is performed for Xc = 0.94. In the classical case and the case with Xc > 1, the attainment of the Poutd power, the possibility of operating in ZVS and the power factor are shown for different coupling coefficients in Table 2. The results for Xc > 1 and Xc < 1.

A first comparison is made under design conditions, with k = kd = 0.155. The output power and IPA φ_1 as a function of switching frequency for k = kd are shown in Fig. 6 (a) and Fig. 6 (b).

Two peaks exceed the rated power in the classical case, which is avoided in the $\mathrm{Xc} \neq 1$ cases. The arrows indicate the points at nominal operation. When several points allow the $\mathrm{Pout_d}$ specification power of 20 kW to be reached, the point that allows operation in ZVS, guarantees the best power factor and avoids passing a power peak is selected.

In the case of over-coupling, i.e. k > kd, the increase of k in front of kd makes it increasingly difficult to meet two important conditions, i.e. operating in ZVS mode and being able to reach Poutd, see Table 2. This is illustrated in particular by Fig. 7 (a) and Fig. 7 (b) for which the coupling coefficient is 0.2. The system is in the classical case at the limit of being able to transfer Poutd while the ZVS mode is no longer possible while transferring Poutd. This is however still possible in the cases Xc < 1 and Xc > 1 as shown in Fig. 7 (a) and Fig. 7 (b).

The maximum coupling coefficients for reaching Poutd and where ZVS mode is possible at Poutd are respectively denoted $\mathrm{k_{Poutd}}$ and $\mathrm{k_{ZVS}}$. As shown in Table 1, the proposed method extends the limits of $\mathrm{k_{Poutd}}$ and $\mathrm{k_{ZVS}}$ by + 67% and + 115% respectively.

Table 1: Maximum coupling to guarantee the ZVS mode at Poutd and to be able to reach Poutd in the classical case and with the proposed method.

	Classical case	Proposed method	Difference
$\mathrm{k_{ZVS}}$	0.18	0.3	+ 67 %
$\mathrm{k_{Poutd}}$	0.2	0.43	+ 115 %

In the under-coupling case where k < kd, the BP and FSP attenuate when the coupling coefficient decreases, as illustrated in the case k = 0.11 Fig. **8** (a) and Fig. 8 (b). The inconvenience of reduced coupling is related to the lower power factor, see table 2.

Table 2: Comparison of WPTS performances in the classical case and with the case A of the proposed method. The capacity to transfer the nominal power $\mathrm{P_{Outd}}$, as well as to operate in ZVS at $\mathrm{P_{Outd}}$ are investigated. The power factor $\cos(\varphi_1)$ is given at $\mathrm{P_{Outd}}$.

	Classical Case			Proposed Method : Case Xc > 1		
	$\mathrm{P_{Outd}}$	ZVS	$\cos(\varphi_1)$	$\mathrm{P_{Outd}}$	ZVS	$\cos(\varphi_1)$
$\mathrm{k} = 0.11$	Yes	Yes	0.66	Yes	Yes	0.72
$\mathrm{k} = 0.13$	Yes	Yes	0.75	Yes	Yes	0.84
$\mathrm{k} = \mathrm{k_d} = 0.155$	Yes	Yes	0.84	Yes	Yes	0.975
$\mathrm{k} = 0.18$	Yes	Boundary	0.99	Yes	Yes	0.986
$\mathrm{k} = 0.2$	Boundary	No	0.975	Yes	Yes	0.99
$\mathrm{k} = 0.3$	No	No	/	Yes	Boundary	0.99
$\mathrm{k} = 0.43$	No	No	/	Boundary	No	0.99

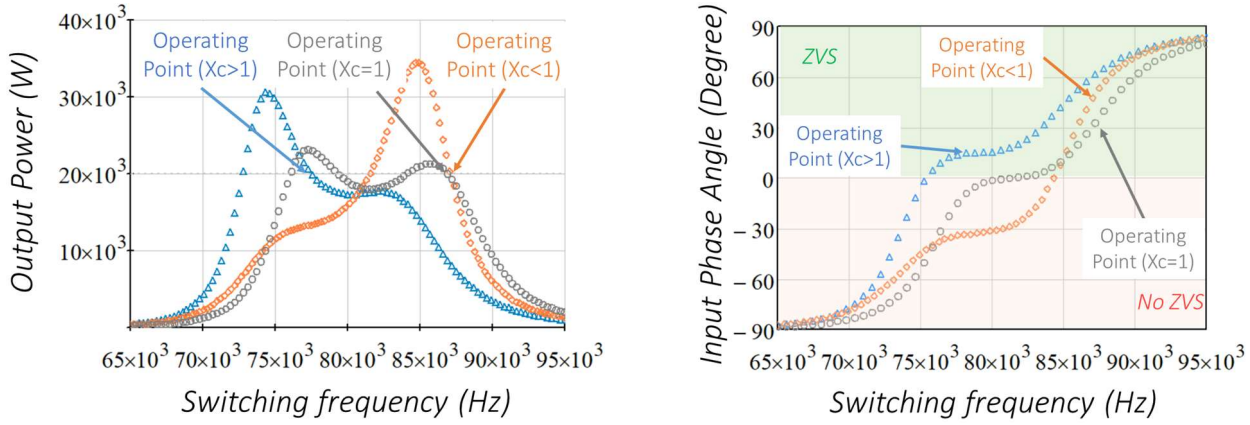

(a) (b)

Fig. 6: Output power (a) and IPA (b) for a coupling coefficient k = 0.155 = kd. Three cases are presented: Xc > 1 (blue), Xc < 1 (orange), and the classical case (grey).

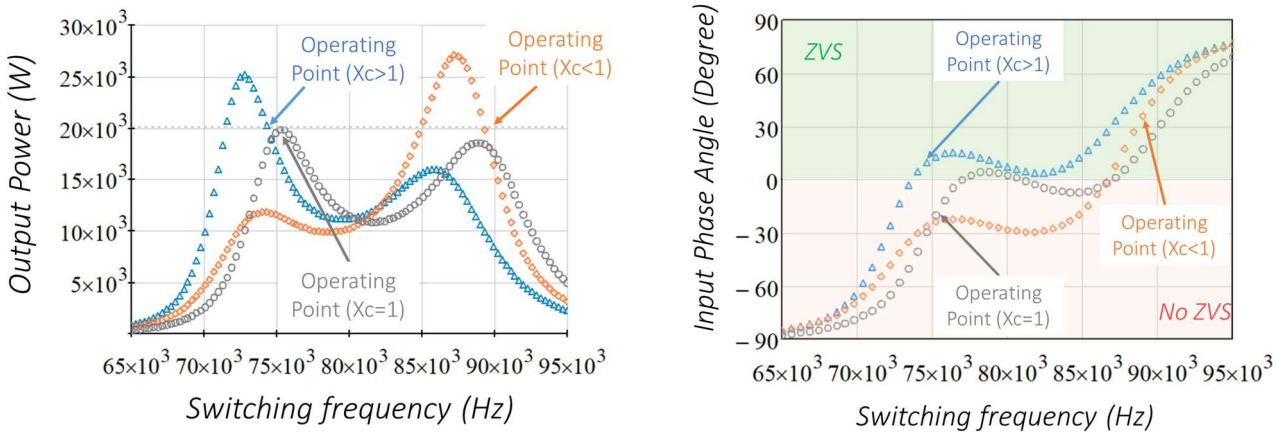

(a) (b)

Fig. 7: Output power (a) and IPA (b) for a coupling coefficient k = 0.2 > kd. Three cases are presented: Xc > 1 (blue), Xc < 1 (orange), and the classical case (grey).

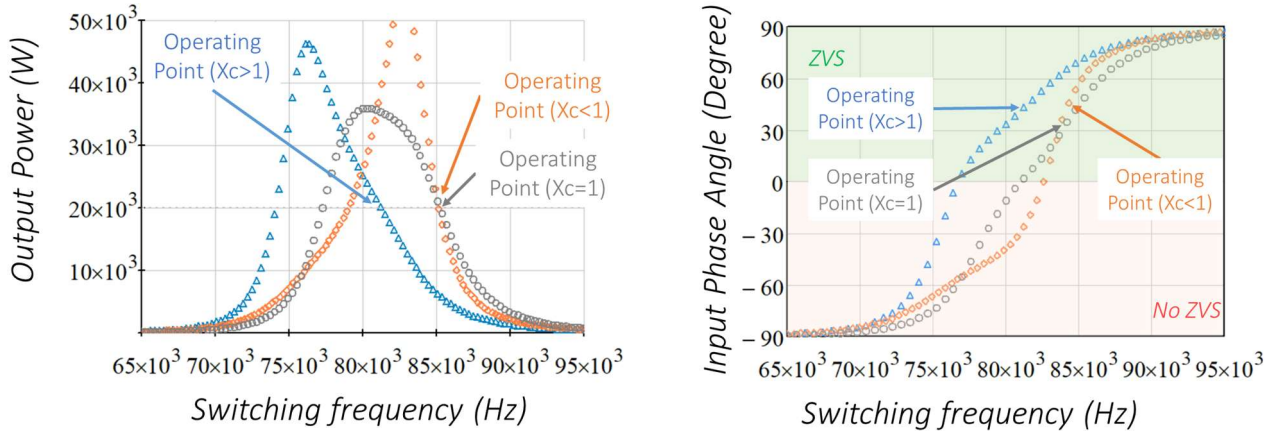

(a) (b)

Fig. 8: Output power (a) and IPA (b) for a coupling coefficient k = 0.11 < kd. Three cases are presented: Xc > 1 (blue), Xc < 1 (orange), and the classical case (grey).

5 Experimental validation

The previous theoretical study is validated in this section through the realisation of a 20 kW WPTS in the case Xc > 1. After presenting the system configuration, the output power versus frequency curve will be compared to the curve with Xc > 1, presented in the theoretical analysis in Fig. 7 (a).

5.1 Setup

The WPTS tested and shown in Fig. 9 has been sized for a nominal power of 20 kW, at a resonant frequency of 81 kHz. Full system characteristics are available in paper [14], [15]. As indicated in section 4.2, the theoretical capacitance values are C1th = 11.40 nF and C2th = 48.86 nF, the selected capacitances are C1c = 12.5 nF and C2c = 50 nF, which corresponds to Xc = 1.041 > 1. This slight difference is sufficient to change the operating point at a given frequency.
The electronics devices used for the measurements are current probes LeCroy CP150, voltage probe LeCroy HVD3605, WaveRunner RO 66Zi 600 MHz oscilloscope and thermal camera.

5.2 Results

The relative error presented in Table 3 is the one between the measured output power of the prototype presented on Fig. 9 and the one calculated from the analytical model. Xc = 1.041 in both cases.
The theoretical and measured output power versus switching frequency curves are shown in Fig. 10. This graph is a zoom between 76 kHz and 83 kHz of Fig. 6 (a) of the blue theoretical curve (with Xc > 1). The relative error between the theoretical and measured values is a maximum of 4.2 % as shown in Table 3. The experimental results thus validate the analytical results presented above.

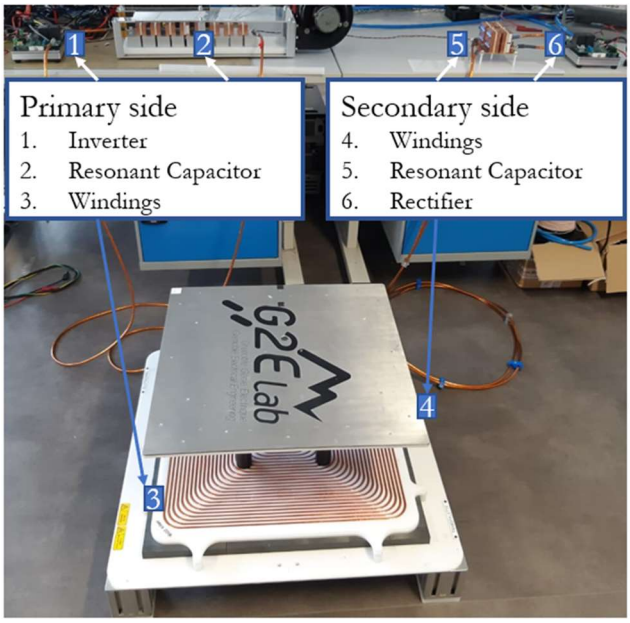

Fig. 9: 20 kW prototype realized with 21 cm air gap.

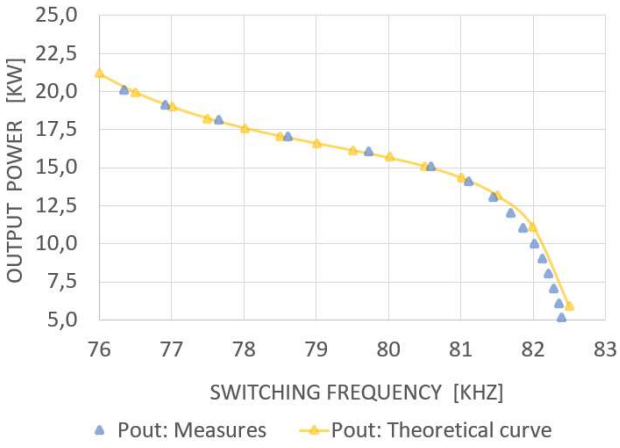

Fig. 10: Comparison of the measured and theoretical output power values between 12 kW and the 20 kW nominal output power in case of Xc = 1.041, for a coupling coefficient k = kd = 0.155.

Table 3: Comparison of the measured and theoretical output power values between 12 kW and the 20 kW nominal output power in case of Xc = 1.041, for a coupling coefficient k = kd = 0.155. The efficiency measured is presented.

Frequency	*Efficiency Measured*	*Pout Measured*	*Pout Th*	*Relative error*
81 688 Hz	*97,1 %*	*12 030 W*	*12 530 W*	*4,2 %*
81 448 Hz	*97,0 %*	*13 037 W*	*13 310 W*	*2,1 %*
81 098 Hz	*97,0 %*	*14 058 W*	*14 140 W*	*0,6 %*
80 568 Hz	*97,0 %*	*15 059 W*	*14 990 W*	*0,5 %*
79 718 Hz	*97,0 %*	*16 062 W*	*15 920 W*	*0,9 %*
78 618 Hz	*96,8 %*	*17 064 W*	*16 940 W*	*0,7 %*
77 638 Hz	*96,6 %*	*18 084 W*	*18 040 W*	*0,2 %*
76 908 Hz	*96,4 %*	*19 091 W*	*19 140 W*	*0,3 %*
76 348 Hz	*96,2 %*	*20 104 W*	*20 260 W*	*0,8 %*

Conclusion

Bifurcation phenomenon (BP) and frequency splitting phenomenon (FSP) frequently appear in WPTS in the case of EV chargers, and are synonymous with additional losses, a control method rendered inoperative, and high sensitivity to the over coupling phenomenon. The impact of an increase in coupling and a decrease in load resistance on the accentuation of bifurcation and frequency splitting phenomena was presented.

An easy to follow proposed method allows to avoid FSP and correct BP by slightly modifying the values of the resonant capacitances during the post-design. In particular, the proposed method makes it possible to reach the nominal power for a coupling coefficient of + 115 % and to maintain the ZVS for an over-coupling of + 67 % compared to the conventional case.

The robustness of the system during coupling and load resistance variations is thus greatly increased without degrading the efficiency thanks to the preservation of a good power factor.

References

[1] A. Namadmalan, B. Jaafari, A. Iqbal, et M. Al-Hitmi, « Design Optimization of Inductive Power Transfer Systems Considering Bifurcation and Equivalent AC Resistance for Spiral Coils », *IEEE Access*, vol. 8, p. 141584-141593, 2020, doi: 10.1109/ACCESS.2020.3013120.

[2] K. N. Mude et K. Aditya, « Comprehensive review and analysis of two-element resonant compensation topologies for wireless inductive power transfer systems », *Chinese Journal of Electrical Engineering*, vol. 5, nº 2, p. 14-31, juin 2019, doi: 10.23919/CJEE.2019.000008.

[3] S. Chopra et P. Bauer, « Analysis and design considerations for a contactless power transfer system », in *2011 IEEE 33rd International Telecommunications Energy Conference (INTELEC)*, oct. 2011, p. 1-6. doi: 10.1109/INTLEC.2011.6099774.

[4] K. Aditya et S. S. Williamson, « Design Guidelines to Avoid Bifurcation in a Series–Series Compensated Inductive Power Transfer System », *IEEE Transactions on Industrial Electronics*, vol. 66, nº 5, p. 3973-3982, mai 2019, doi: 10.1109/TIE.2018.2851953.

[5] M. Košík, R. Fajtl, et J. Lettl, « Analysis of bifurcation in two-coil inductive power transfer », in *2017 IEEE 18th Workshop on Control and Modeling for Power Electronics (COMPEL)*, juill. 2017, p. 1-8. doi: 10.1109/COMPEL.2017.8013324.

[6] S. Moon, B.-C. Kim, S.-Y. Cho, C.-H. Ahn, et G.-W. Moon, « Analysis and Design of a Wireless Power Transfer System With an Intermediate Coil for High Efficiency », *IEEE Transactions on Industrial Electronics*, vol. 61, nº 11, p. 5861-5870, nov. 2014, doi: 10.1109/TIE.2014.2301762.

[7] W.-Q. Niu, J.-X. Chu, W. Gu, et A.-D. Shen, « Exact Analysis of Frequency Splitting Phenomena of Contactless Power Transfer Systems », *IEEE Transactions on Circuits and Systems I: Regular Papers*, vol. 60, nº 6, p. 1670-1677, juin 2013, doi: 10.1109/TCSI.2012.2221172.

[8] H. Kim *et al.*, « Mitigation of Frequency Splitting Phenomena Using a Matching Capacitor in Wireless Power Transfer System for Automated Guided Vehicle », in *2020 IEEE Wireless Power Transfer Conference (WPTC)*, nov. 2020, p. 170-173. doi: 10.1109/WPTC48563.2020.9295565.

[9] B. D. Truong, « Further Results on “Design Guidelines to Avoid Bifurcation in a Series–Series Compensated IPTS”: Theoretical Analysis and Experimental Validations », *IEEE Transactions on Industrial Electronics*, vol. 68, nº 4, p. 3643-3648, avr. 2021, doi: 10.1109/TIE.2020.2978715.

[10] J.-P. Ferrieux *et al.*, « Maximising transferred power and preserving zero voltage switching in grid to vehicle and vehicle to grid modes of a wireless charging system », *IET Electrical Systems in Transportation*, vol. 10, nº 2, p. 196-203, 2020, doi: 10.1049/iet-est.2018.5079.

[11] C. Wei, D. Zhu, H. Xie, Y. Liu, et J. Shao, « A SiC-Based 22kW Bi-directional CLLC Resonant Converter with Flexible Voltage Gain Control Scheme for EV On-Board Charger », in *PCIM Europe digital days 2020; International Exhibition and Conference for Power Electronics, Intelligent Motion, Renewable Energy and Energy Management*, juill. 2020, p. 1-7.

[12] Chwei-Sen Wang, G. A. Covic, et O. H. Stielau, « Power transfer capability and bifurcation phenomena of loosely coupled inductive power transfer systems », *IEEE Transactions on Industrial Electronics*, vol. 51, nº 1, p. 148-157, févr. 2004, doi: 10.1109/TIE.2003.822038.

[13] N. Hatchavanich, A. Sangswang, et M. Konghirun, « Secondary-Side Voltage Control via Primary-Side Controller for Wireless EV Chargers », *IEEE Access*, vol. 8, p. 203543-203554, 2020, doi: 10.1109/ACCESS.2020.3036542.

[14] B. Sarrazin, A. Derbey, P. Albouy, J.-P. Ferrieux, G. Meunier, et J.-L. Schanen, « Bidirectional Wireless Power Transfer System with Wireless Control for Electrical Vehicle », in *2019 IEEE Applied Power Electronics Conference and Exposition (APEC)*, Anaheim, CA, USA, mars 2019, p. 3137-3143. doi: 10.1109/APEC.2019.8721800.

[15] D. Lemaitre, B. Sarrazin, Y. Wanderoild, Y. Lembeye, et A. Derbey, « Efficiency-Oriented Design of Litz Wire for Several kW Power Experimented on 20 kW Prototype », in *PCIM Europe digital days 2021; International Exhibition and Conference for Power Electronics, Intelligent Motion, Renewable Energy and Energy Management*, mai 2021, p. 1-8.